Computational Study of a Single-Phase Flow in Packed Beds of Spheres

Prashant R. Gunjal, Vivek V. Ranade, and Raghunath V. Chaudhari
Industrial Flow Modeling Group, Homogeneous Catalysis Division, National Chemical Laboratory, Pune 411008, India

DOI 10.1002/aic.10314
Published online in Wiley InterScience (www.interscience.wiley.com).

Packed-bed reactors are widely used in petrochemical, fine chemical, and pharmaceutical industries. Detailed knowledge of interstitial flow in the void space of such packed-bed reactors is essential for understanding the heat and mass transfer characteristics. In this paper, fluid flow through the array of spheres was studied using the unit-cell approach, in which different periodically repeating arrangements of particles such as simple cubical, 1-D rhombohedral, 3-D rhombohedral, and face-centered cubical geometries were considered. Single-phase flow through these geometries was simulated using computational fluid dynamics (CFD). The model was first validated by comparing predicted results with published experimental and computational results. The validated model was further used to study the effect of particle arrangement/orientation on velocity distribution and heat transfer characteristics. The simulated results were also used to understand and to quantify relative contributions of surface drag and form drag in overall resistance to the flow through packed-bed reactors. The model and the results presented here would be useful in elucidating the role of microscopic flow structure on mixing and other transport processes occurring in packed-bed reactors. © 2005 American Institute of Chemical Engineers *AIChE J,* 51: 365–378, 2005
Keywords: packed bed, CFD, packing arrangement, drag, heat transfer

Introduction

Single- or two-phase flow through a packed bed of spheres occurs in many chemical process industries. Flow through complex interstitial geometry formed by bed particles controls mixing and other transport processes occurring in a packed bed. Several experimental and computational studies have thus been carried out to understand flow through the voids of packed beds. Most of the previous studies were restricted to understand the global parameters such as pressure drop, drag force exerted on particles, and overall voidage of bed. However, spurred by new developments in experimental as well as theoretical/computational techniques, it is now possible to gain detailed insight into the packed bed to tailor, monitor, and optimize the performance. Recent advancements in experimental techniques such as MRI provide detailed information about the flow field (for example, Sederman and Gladden, 2001; Sederman et al., 1997; Suekane et al., 2003). However, it is difficult to study the influence of all the key parameters extensively only by experiments. Instead it will be more effective to use such comprehensive data sets to validate computational models and use the validated models for further investigations. Therefore, several attempts have recently been made to develop computational models for simulating flow in packed beds (see, for example, Calis et al., 2001; Dixon and Nijemeisland, 2001; Freund et al., 2003; Logtenberg et al., 1999; Tobis, 2000; Zeiser et al., 2002).

Computational studies mainly used two approaches. In the first approach, the entire packed bed, consisting of number of particles (arranged in either a regular fashion or a random fashion), is considered. Logtenberg et al. (1999), Nijemeisland and Dixon (2001), Calis et al. (2001), and Nijemeisland and Dixon (2004), among others, have used this approach. Computational constraints often limit the size of the bed and number of particles considered in such simulations. For simulating flow

Correspondence concerning this article should be addressed to V. V. Ranade at vvranade@ifmg.ncl.res.in.

in large packed beds, therefore, often the second approach, called the "unit-cell approach," is used. There are two subtypes in the unit-cell approach. In the first type, each particle is assumed to have a hypothetical sphere of influence around it (see Dhole et al., 2004 and references cited therein). Flow is solved around a particle placed in a hypothetical sphere of influence (the size of which depends on porosity of the bed). This approach, however, ignores differences caused by different particle arrangements and therefore was not used in the present work. In the second type of unit-cell approach, a unit "periodic" cell consisting of only a few particles is considered. The packed bed is represented by periodically repeating the unit cell in all three directions. This approach is being used traditionally to analyze transport processes in packed beds (see, for example, Martin et al., 1951, Sørensen and Stewart, 1974). Different packing arrangements of particles, such as simple cubic (SC), rhombohedral, and face- or body-centered cubic (FCC or BCC), can be considered for representing the packed bed. This approach is used in the present work.

Depending on the flow rates, properties of fluids and loading of solid, different types of flow patterns were observed by several authors (Hill et al., 2001; Seguin et al., 1998a,b). At very low flow rates, creeping flow exists, such that $Re_p < 1$, where Re_p is the particle Reynolds number based on mean velocity in the void space ($Re_p = \rho U_0 d_p/\varepsilon\mu$); the inertial flow regime begins above $Re_p = 10$. This inertial flow regime extends up to $Re_p = 250–350$. With further increase in Reynolds number, the transition flow regime (unsteady flow) occurs up to $Re_p = 900$ (Seguin et al., 1998b). The transition of flow regime from laminar to turbulent flow in packed beds is difficult to identify and it occurs over a range of Reynolds number. The occurrence of transition to turbulence is a complex function of size and shape of particles and bed-packing characteristics. Previous studies (for example, Chhabra et al., 2001; Seguin et al, 1998 a,b) indicate that beyond $Re_p = 350$, flow is dominated by eddies and turbulent-like structures. Seguin et al. (1998b) experimentally showed that turbulent flow exists beyond $Re_p = 900$. Jolls and Hanratty (1966) and Latafi et al. (1989) reported that transition occurs at over the range of $Re = 300–400$ ($Re = \rho U_0 d_p/\mu$). Based on these studies it can be assumed that flow becomes turbulent beyond a particle Reynolds number of 1000.

Sangani and Acrivos (1982) and Sørensen and Stewart (1974) previously analyzed flow through unit cells with particles arranged in SC and FCC patterns. They reported the drag force exerted on particles at different values of porosity, although their study was limited to the Stokes flow regime ($Re \rightarrow 0$). The Stokes flow regime exists at very low particle Reynolds number ($\lesssim 0.1$), where the average drag force on particles is independent of Reynolds number. Considering the usual operating ranges of packed beds, it is essential to understand the flow characteristics in the inertial flow regime (particle Reynolds number > 10). Only recently have some attempts been made to analyze inertial flow in packed beds.

Durst et al. (1987) simulated laminar flow through unit cells and compared simulated pressure drop with experimental data. Details of simulated flow field were neither discussed nor validated. Maier et al. (1998) carried out lattice–Boltzmann simulations of single-phase flow through FCC and random-packing arrangement of particles. They presented some comparisons of simulated velocity distribution with their experimental results. Their study was restricted to low Reynolds number ($Re = 0.5–29$). Tobis (2000) used a unit-cell approach for simulating turbulent flow in a packed bed, although detailed flow characteristics and velocity profiles were not discussed. Hill et al. (2001a) carried out the lattice–Boltzmann simulations of flow through FCC, SC, and random arrangement of particles. Detailed analysis of drag force variation with solid volume fraction and packing arrangement was discussed. Freund et al. (2003) carried out lattice–Boltzmann simulations of flow in a packed-bed reactor of low-aspect ratio (~ 5). They studied the relative contributions of viscous and form drag in overall pressure drop. Detailed analysis of flow structure in a packed bed, velocity distribution, and its effect on transport properties is needed. Recently, Magnico (2003) carried out simulations for a unit cell and for small tube-to-sphere diameter ratio for the range of Reynolds numbers from 7 to 200. He demonstrated the influence of flow structures on mass transfer with the help of Lagrangian particle tracking. Despite these modeling efforts, none of the flow simulations (except the attempt by Freund et al., 2003) was validated by comparison with experimental data. Most of the studies were restricted to comparison with the overall pressure drop. If the computation models are validated by detailed comparison with the experimental data, such models can be used to understand the influence of Reynolds number and particle arrangement on flow structures and therefore on transport processes in packed beds.

Detailed experimental data of flow through packed beds are now available. Sederman et al. (1997), Sederman and Gladden (2001), and Mantle et al. (2001) experimentally characterized the flow in packed beds and reported measured distributions of axial and transverse velocities in interstitial space. The axial velocity distribution showed a sharp decay and was asymmetrical. The transverse velocity distribution showed exponential decay in both positive and negative directions. Experimental data reported by Maier et al. (1998) also show similar trends of velocity distributions. Recently, Suekane et al. (2003) carried out detailed measurements of flow through voids of a simple packed bed using magnetic resonance imaging (MRI) and have provided detailed quantitative data. They also reported details of inertial flow structures for different Reynolds numbers. In this paper, we have used their experimental data to evaluate our computational model.

The computational model was developed to simulate flow in unit cells of particles with SC, rhombohedral, and FCC arrangements. Simulated results were compared with the experimental data for Suekane et al. (2003) for SC in a laminar flow regime. The effects of grid and grid size distribution and other numerical parameters such as discretization schemes and conversion criteria were discussed. Computational fluid dynamics (CFD) model results were also compared with the analytical solution (given by Sangani and Acrivos, 1982) at low Reynolds number ($Re = 0.001$), and with the simulated results of Hill et al. (2001a) and Dhole et al. (2004) at moderate Reynolds numbers ($Re_p = 10–500$). The validated computational model was used to understand the influence of packing arrangement of particles on flow structure using different packing arrangements such as FCC and rhombohedral. Detailed comparisons of flow fields of cubical, FCC, and rhombohedral geometry were presented for a wide range of Reynolds numbers (12–2000). Axial and transverse velocity distributions in a unit cell were compared with the velocity distribution in a randomly

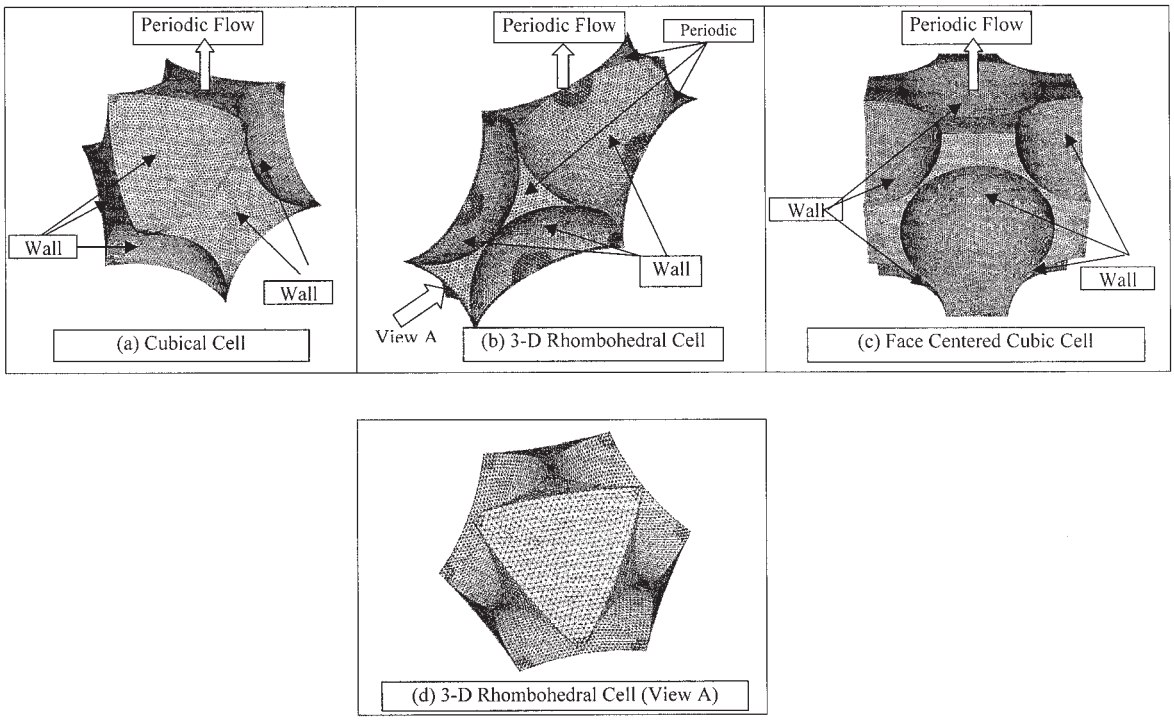

Figure 1. Domain, computational grid, and boundary conditions.

packed bed. The simulated results were also used to quantify the relative contributions of shear drag at the wetted area and form drag in overall pressure drop. The effect of flow structure on particle to fluid heat transfer coefficient was studied with the help of this CFD model. The models and results discussed here would be useful for enhancing our understanding of flow through packed beds.

Computational Model

The approach of unit cells, where packed bed of spheres is represented by geometrically periodic unit cells with different packing arrangements, is advantageous in understanding flow structures in large packed beds; however, it is essential to understand possible implications of approximating a packed bed by periodic unit cells. It is well known that symmetry of a flow over a single sphere breaks when particle Reynolds number increases beyond 105 and unsteady flow occurs (Natarajan and Acrivos, 1993). The unit-cell approach is not valid for cases where periodic symmetry of flow is absent, despite the symmetric and periodic geometry. Fortunately, when particles are packed closely together in a regular fashion, the onset of symmetry breaking unsteady flow is delayed considerably (Hill et al., 2001a). The largest length scale characterizing the interstitial region of the regular arrays is smaller than the particle diameter. Therefore the Reynolds number characterizing the stability of the flow in the interstitial region can be up to about 2.5-fold larger than the critical particle Reynolds number. Second, at larger solid volume fractions, the fluid is increasingly confined and is thus stabilized by neighboring spheres. For a specific particle Reynolds number, viscous dissipation will be higher at higher solid volume fraction, and therefore more effective in damping velocity fluctuations. Considering this, in the present work, the unit-cell approach was used to understand the influence of particle Reynolds number and packing arrangement on inertial flow structures in packed beds.

In this work, different packing arrangements of spheres [that is, SC, one-dimensional (1-D) and three-dimensional (3-D) rhombohedral, and FCC] were considered. These are shown in Figure 1. In the first part of the present work, a unit cell consisting of four spheres in a simple cubical arrangement (ε = 0.4764) was selected to facilitate comparison of the simulated results with the experimental data of Suekane et al. (2003). To study the effect of particle arrangements, flow simulations of unit cells with 1-D rhombohedral arrangement (ε = 0.4525), 3-D rhombohedral (ε = 0.2595), and face-centered cubical (FCC) arrangement (ε = 0.302) were carried out. Simulations were also carried out for SC and FCC arrangements with different porosity to understand the influence of solid fraction on velocity distribution.

The geometry of interstitial space of these unit cells was modeled using GAMBIT 2.0 software (Fluent USA, Lebanon, NH). Unstructured tetrahedral grids were generated as shown in Figure 1. For the SC and FCC unit cells, only one fourth of the domain shown in Figures 1a–c was used for flow simulations because of the inherent symmetry. For the rhombohedral unit cell (3-D), however, complete geometry as shown in Figure 1b was used for flow simulations. Different computational grids were generated to quantify the influence of grid size on the predicted results. These results are discussed in the next section.

Three-dimensional Navier–Stokes equations were used to simulate the laminar flow of an incompressible fluid through a packed bed of spheres. The simulated results were compared with the experimental results of Suekane et al. (2003). The

predicted flow results were used to simulate particle-to-fluid heat transfer by solving the enthalpy balance equation. Although the experimental study of Suekane et al. (2003) was limited to particle Reynolds number up to 204.74, it was thought desirable to use the computational model to understand flow characteristics for particle Reynolds number beyond the laminar range. The study of Seguin et al (1998a,b) indicated that the flow in a packed bed exhibits a transition regime over a large range of particle Reynolds numbers and the turbulent flow regime may exist beyond $Re_p = 900$. Considering the uncertainties in simulating transition flow regime in a complex geometry, some simulations of the flow in packed beds were carried out for a turbulent regime (particle Reynolds numbers of 1000 and 2000). For these cases, Reynolds-averaged Navier–Stokes equations (and enthalpy equation) were used along with the standard k–ε model of turbulence. In a laminar flow regime, turbulent stresses were neglected, whereas in the turbulent flow regime turbulent stresses were accounted for in the model. Details of governing equations and boundary conditions are given in the Appendix.

Simulations of flow (and heat transfer) were carried out using the commercial CFD solver FLUENT (version 6.1.18; Fluent USA). The underrelaxation parameters for pressure and velocity were set to 0.05 and 0.1, respectively, at the start and were increased up to 0.2 and 0.3 as the solution progressed. For turbulent flow, underrelaxation parameters for turbulent kinetic energy, dissipation rate, and turbulent viscosity were used as 0.25, 0.25, and 0.6, respectively. Numerical issues and grid independence of solution are discussed in the following sections. Simulations were carried out until the normalized residuals fall below 1×10^{-6} (1×10^{-7} for energy equations) for all the equations. For every simulation, it was ensured that pressure drop per unit length remained constant for several subsequent iterations. Simulations were first carried out with operating parameters used exactly like those used in the experiments of Suekane et al. (2003). The validated model was then used to study flow over a wide range of the particle Reynolds numbers (12–2000) over different packing arrangements.

Results and Discussion

In the first section we have compared predictions of the CFD model with the available experimental as well as analytical/computational results. In the second section, the results on influence of particle Reynolds number and of particle arrangement on flow are discussed. Drag force acting on the particles and contribution of viscous drag in total drag is discussed after that. Finally, results pertaining to the effect of particle arrangement and flow characteristics on wall to particle heat transfer coefficient are presented.

Validation of CFD model

The predictions of the CFD model were first compared with the experimental data of Suekane et al. (2003), measured using MRI technique for different particle Reynolds numbers (12.17–204.74). The model predictions were also compared with the analytical solutions presented by Sangani and Acrivos (1982) at the limit of vanishing Reynolds number (<0.01). The simulated results of the present work were also compared with the predicted results of Hill et al. (2001) and Dhole et al. (2004). These results are discussed in the following.

Comparison with Experimental Data of Suekane et al. (2003). Suekane et al. (2003) carried out detailed measurements of flow through an array of spheres over the range of particle Reynolds numbers 12 to 205. They reported velocity profiles and details of secondary flow structures for five particle Reynolds numbers (12.17, 28.88, 59.78, 105.5, and 204.74). Because the scatter in the reported experimental data was much lower for the case of Reynolds number of 204.74 (compared to that for the lower values of Reynolds number), this case was selected for critical evaluation of the computational model. Several numerical experiments were carried out to understand the effects of grid size, distribution, and discretization schemes. Preliminary simulations were performed with different numbers of computational cells (33K, 112.5K, and 287.5K). Simulated results obtained with different discretization schemes and different computational cells are compared with the experimental data in Figure 2. When a second-order discretization scheme was used, the predicted results with 112.5K and 287.5K computational cells were almost the same. All the subsequent simulations were thus carried out using a second-order discretization scheme and the total number of computational cells was >150K.

After establishing the adequacy of computational parameters, simulations were carried out for five values of Reynolds numbers considered by Suekane et al. (2003). The highest Reynolds number considered in the experiments was 204.74. From previous literature (Chhabra et al., 2001; Seguin et al., 1998) it was found that flow at this Reynolds number is laminar and thus the laminar flow model was used to simulate these cases. Comparison of simulated velocity field (vectors) with the experimental data is shown in Figure 3. It can be seen that variation of axial velocity was well captured in the simulated results. At the highest Reynolds number ($Re_p = 204.74$), where inertial forces are dominant, jetlike flow behavior was observed in the experimental flow fields (see Figure 3c). A similarly dominant velocity stream through the center of the solution domain was also observed in the simulation. Quantitative comparison of the simulated and the measured z-component of the velocity is shown in Figure 4. Simulated results showed good agreement with the experimental data, except at the lowest value of Reynolds number (12.17).

Systematic numerical experiments were carried out to understand possible reasons for the observed discrepancies at low Reynolds number. Influences of the number of computational cells, the distribution of cells within the solution domain, and the discretization scheme were insignificant as long as the total number of computational cells is >150K. Another possible source can be round-off errors. At lower values of Reynolds number, the mass flow through the unit cell becomes quite small if viscosity of the considered fluid is waterlike. To examine this, all the simulations were carried out using a double-precision solver. Simulations were also carried out by selecting physical properties of fluid in such a way that the mass flow rate at the desired value of particle Reynolds number is too small to be influenced by round-off error. These numerical experiments indicated that the observed discrepancies at $Re_p = 12.17$ are not attributed to numerical errors. It is interesting to note that experimental results also show the highest scatter at this particle Reynolds number. Possible difficulties in maintaining a steady flow at a very low flow rate may be one of the reasons for such scatter. To examine this further; flow

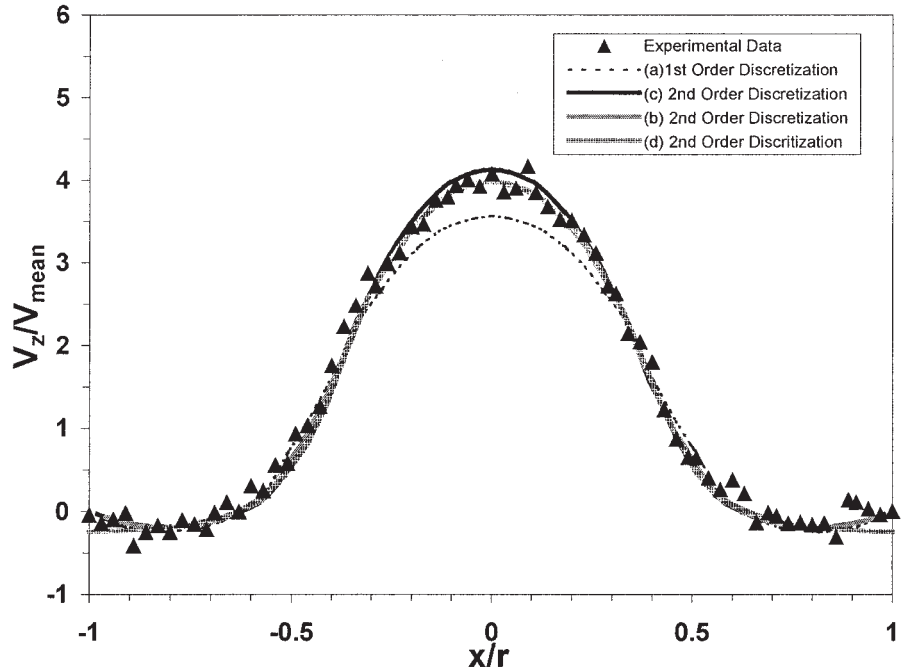

Figure 2. Effect of numerical parameters on *z*-velocity distribution along the *x*-axis at the highest cross-sectional area at $y = 0.0015$ and $Re = 204.74$.

simulations were carried out with particle Reynolds numbers of 10.95 (10% lower flow) and 9.12 (25% lower flow). These results are compared with the experimental data reported at $Re_p = 12.17$ in Figure 4. It can be seen that the reported experimental data lie between the predicted results for Re_p values of 9.12 and 10.95.

Simulated results of flow field variation along the flow direction at three horizontal planes were compared with the experimental data in Figure 5 (for $Re_p = 59.78$) and in Figure 6 (for $Re_p = 204.74$). At low Reynolds number ($Re_p = 59.78$), flow directions normal to the walls of sphere are different for planes A and C. At plane A, the fluid moves toward the walls of the sphere, whereas at plane C, the fluid appears to move away from walls of the sphere. The computational model captured this experimental observation very well. At higher Reynolds number ($Re_p = 204.74$; Figure 6), a pair of vortices was observed in experimental measurements carried out at plane A. These vortices were also captured very well in the simulations (see Figure 6a). It is noteworthy that at higher Reynolds number (204.74), the observed and simulated flow at plane C are qualitatively different from that observed at lower Reynolds number (59.78). Figures 2 to 6 indicate very good overall agreement between the simulated and the experimental results. Simulated results not only showed good agreement with the data in the main flow direction but also correctly captured inertial flow structures. The computational model was then used to understand the effects of particle Reynolds number and packing arrangement of spheres on key flow characteristics.

Comparison of Results with Analytical Solution. Sangani and Acrivos (1982) presented analytical solutions for flow through regular particle arrangements such as SC and FCC at vanishing Reynolds number ($Re_p \rightarrow 0$). At low Reynolds numbers, the dimensionless drag force on particles

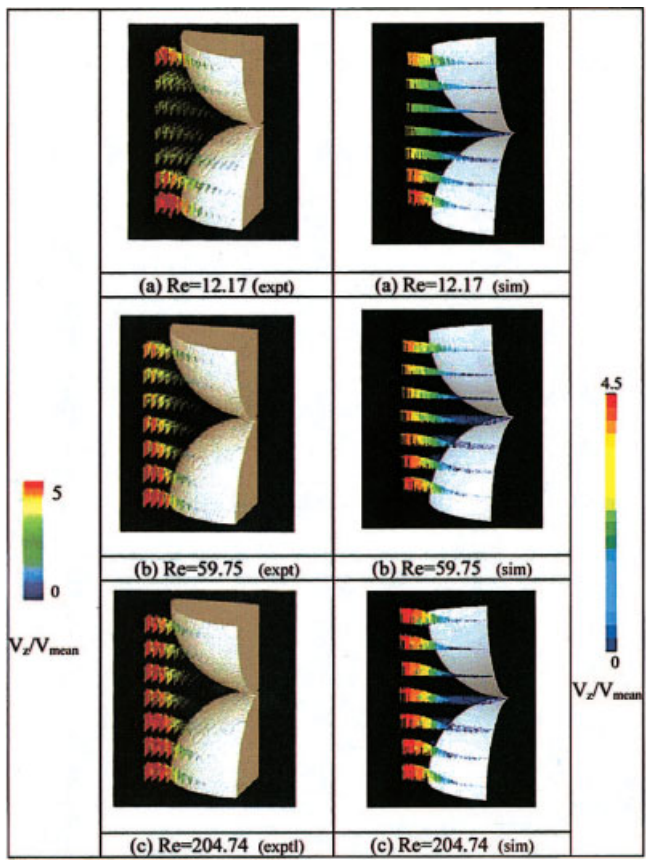

Figure 3. Comparison of simulated results of *z*-velocity with experimental data (Suekane et al., 2003) at different particle Reynolds numbers.

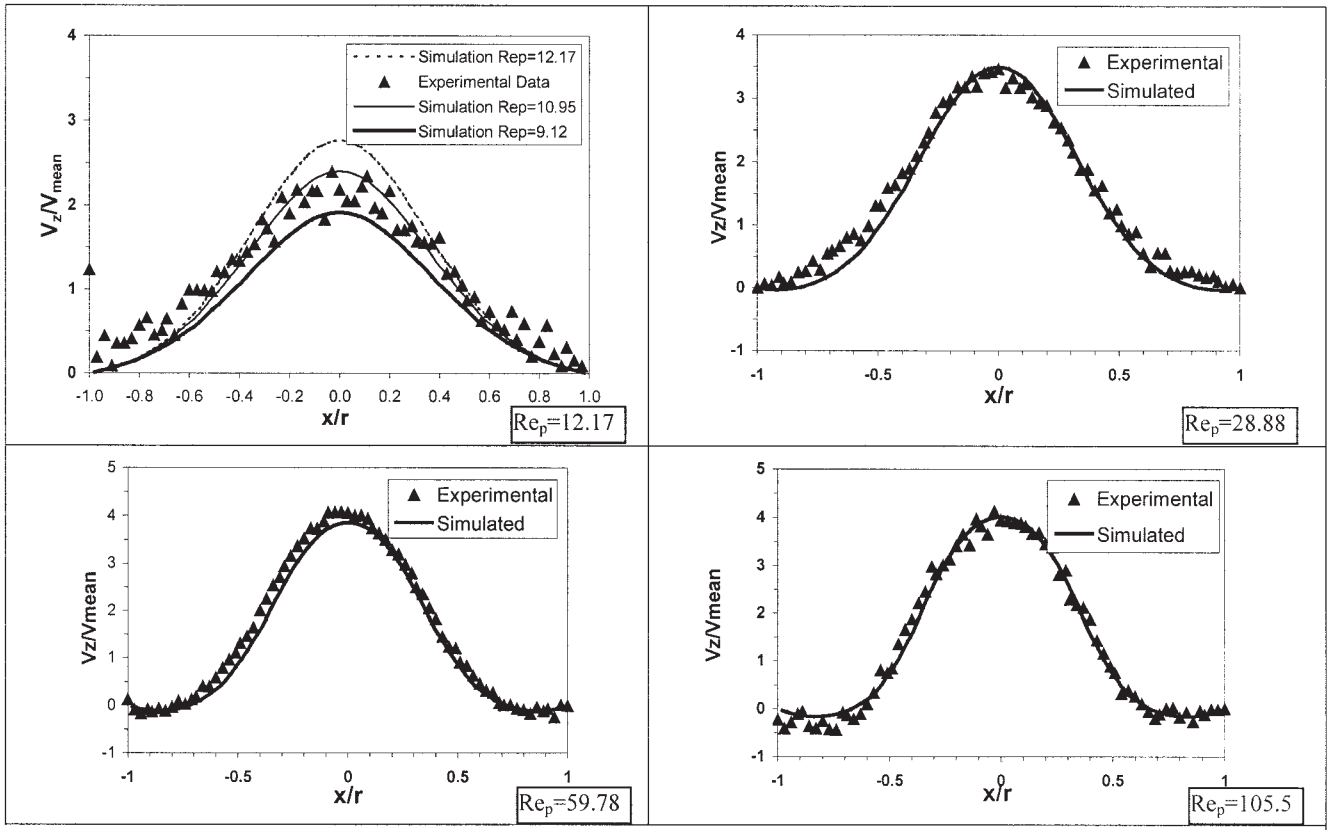

Figure 4. Comparison of simulated *z*-velocity distribution with experimental data at various Reynolds numbers.

Velocity measured at z midplane along the x-axis at $y = 0.0015$.

$[F/(6\pi\mu RV)]$ is independent of Reynolds number and is a function of solid fraction (see Hill et al., 2001; Sangani and Acrivos, 1982). Hill et al. (2001 carried out lattice–Boltzmann (LB) simulations and showed that the analytical solution given by Sangani and Acrivos (1982) matches well with their LB simulations at low solid volume fractions. To compare our computational results with the analytical solution and with the lattice–Boltzmann simulations of Hill et al. (2001), we carried out simulations for low Reynolds number ($Re_p = 0.001$) with FCC geometry. Predictions of our model are compared with the previous results of Sangani and Acrivos (1982) and Hill et al. (2001) in Figure 7a. It can be seen that our simulated results agree quite well with the results of LB simulations of Hill et al. (2001) and both results are in substantial agreement with the analytical solution at low solid volume fraction.

Comparison of Results with those of Hill et al. (2001a) and Dhole et al. (2004). In this section, predicted values of the average drag force acting on particles are compared with the results of Hill et al. (2001b) and Dhole et al. (2004) for moderate values of particle Reynolds numbers. Hill et al. (2001) carried out lattice–Boltzmann simulations for FCC geometry for a range of particle Reynolds numbers 40 to 500, whereas the approach used by Dhole et al. (2004) is independent of particle arrangement. Results are presented in terms of drag coefficient, defined as

$$C_d = \frac{2F_D}{\rho V^2 \pi R^2} \tag{1}$$

The predicted drag coefficients for FCC and SC geometry with solid volume fraction equal to 0.5 are shown in Figure 7b. It can be seen from Figure 7b that the results of our model agree reasonably well with the published results.

Despite some discrepancies seen in Figure 4 (for $Re_p = 12.17$), the overall results of our computational model can be said to be in good agreement with the experimental as well as previous computational results over a broad range of particle Reynolds numbers. The effects of particle arrangement on velocity distribution, drag force, and heat transfer are discussed in the following after discussing the influence of particle Reynolds number on flow structure.

Influence of Reynolds number

Simulations were carried out for higher Reynolds number (that is, Re_p values of 1000 and 2000) to study the influence of Reynolds number on velocity distribution, drag forces, and heat transfer. Only the effect of turbulence flow field in SC geometry is discussed here and the effects of other parameters such as turbulence on particle arrangement, drag force, and heat transfer are discussed in the next respective sections.

Simulated results show that the maximum in profiles of normalized axial velocities increases with increasing Reynolds number for the laminar flow regime ($Re_p = 12.17$–204.74; Figures 4a–d). However, for the turbulent regime (Re_p values of 1000 and 2000), the normalized profiles are almost independent of Reynolds number. The maximum value of normalized velocity is closer to that obtained with the lowest Reynolds

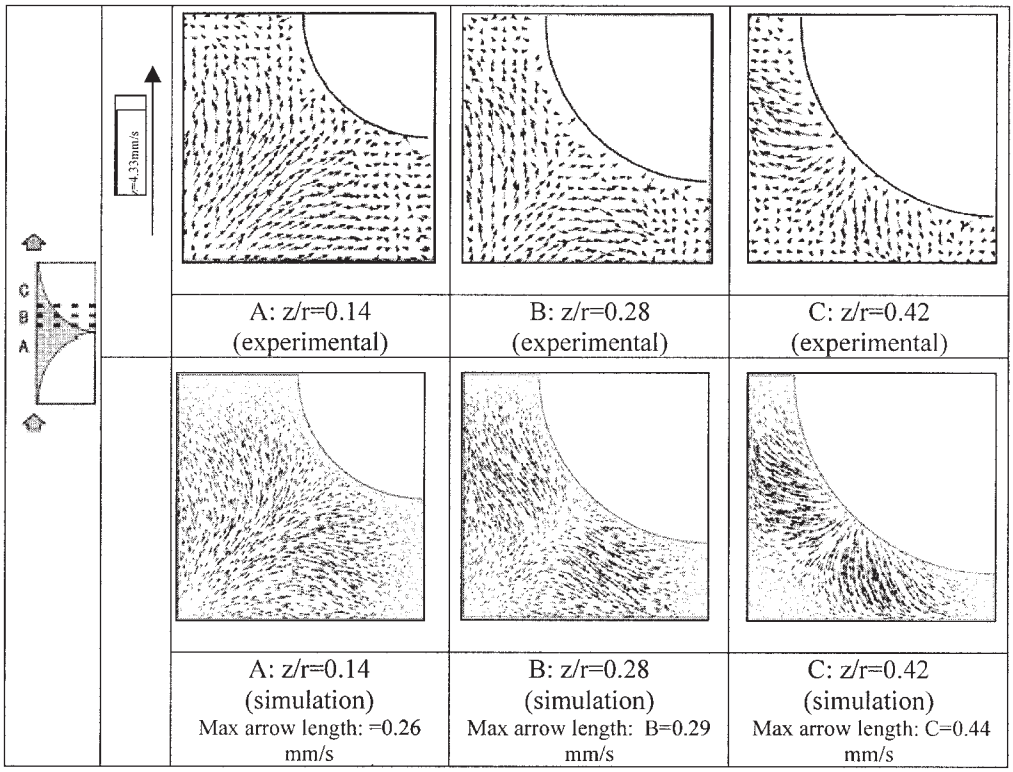

Figure 5. Comparison of the simulated flow field with experimental data at three horizontal planes (Suekane et al., 2003) at Re_p = 59.78.

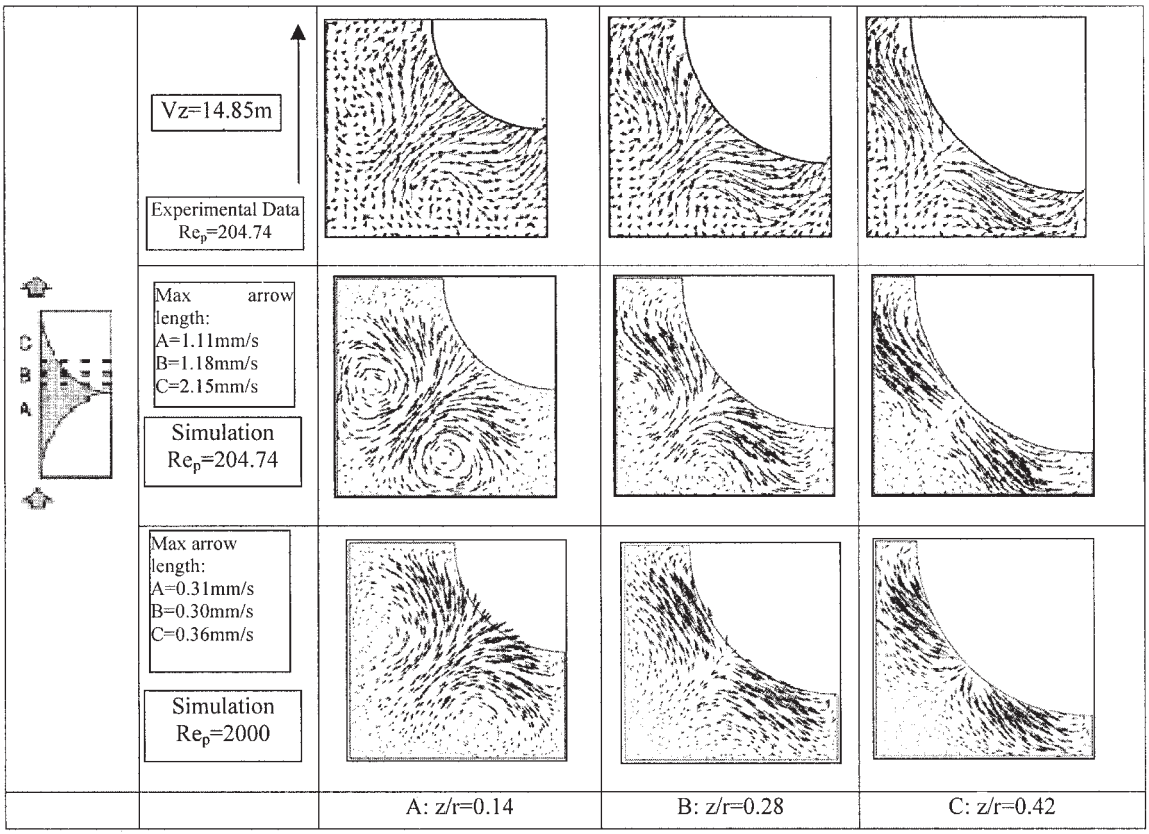

Figure 6. Comparison of the simulated flow field with experimental data at three horizontal planes.

Re_p = 204.74 and 2000.

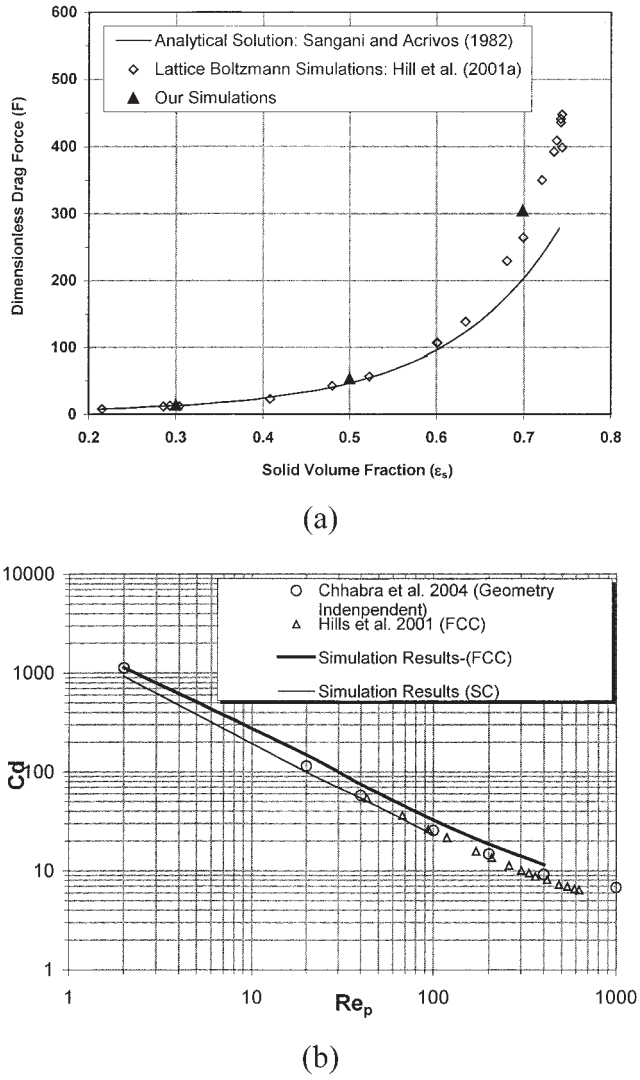

Figure 7. (a) Comparison of simulated results with the literature data for low Reynolds number (Re_p = 0.001); (b) comparison of simulated average drag coefficient with the literature data at various Reynolds numbers.

number considered in the laminar regime (Re_p = 12.17). Velocity profiles for the turbulence cases are much flatter than those obtained for the laminar regime. The region of negative velocities near the wall was found to be larger in turbulent flow regime compared to the laminar regime.

A detailed comparison of the predicted results for the turbulent flow regime with experimental data is not possible because of the lack of available data. Velocity vectors in transverse planes (planes A, B, and C) are shown in Figure 6. A pair of symmetric vortices was observed at plane A for particle Reynolds number of 2000, which was similar to that observed at particle Reynolds number of 204.74. At plane B, flow characteristics obtained for Reynolds number of 2000 were qualitatively similar to those observed at Re_p values of 59.78 and 204.74 (see Figures 5C and 6A and B). At plane C, the flow pattern observed for Re_p = 2000 was found to be similar to that observed for Re_p = 59.78 (that is fluid appears to move away from the walls of the sphere). Knowledge of such detailed flow structure within void spaces will have significant implications for estimation of heat and mass transfer. The effects of particle orientation and flow structures on velocity distribution are discussed in the following section.

Influence of packing arrangement

To understand the influence of packing arrangement of particles in a unit cell, simulations were carried out for different particle arrangements: 1-D rhombohedral (ε = 0.4547), 3-D rhombohedral (ε = 0.2595), and face-centered cubic (ε = 0.302) arrangements. Simulations were carried out at different particle Reynolds numbers in a laminar flow regime (Re_p = 12.17–204.74) and in a turbulent flow regime (Re_p values of 1000 and 2000).

For the 1-D rhombohedral arrangement the predicted velocity field at different particle Reynolds numbers is shown in Figure 8. It can be seen that flow at lower Reynolds number (12.17 and 59.78) is qualitatively different from that at higher Reynolds numbers (204.74 and 2000). At higher Reynolds number, the wake behind the spheres divides the high-velocity stream into two parts at periodic planes (see two groups of red vectors in Figures 8c and d). Profiles of the predicted normalized z-component of the velocity on periodic plane at x = 0.0015 are shown in Figure 8e. At lower Reynolds number (Re_p = 12.17), the flow profile is a bell shape with maximum velocity about twice the mean velocity ($V_{max} = 2V_m$). With increase in Reynolds number the flow profile becomes flattened and the wake behind the solid body starts to affect the flow profiles. At Re_p = 2000, splitting of the high-velocity stream into two parts is obvious from the velocity profiles, shown in Figure 8e. Comparison of Figure 8e and Figure 4 clearly demonstrates the influence of packing arrangement on flow in interstitial spaces. It can be seen from Figure 4 that for a simple cubical (SC) arrangement the ratio of the z-component of velocity and the mean velocity is 2.5 for the lowest Reynolds number and increases up to 4 with increase in Reynolds number. For the rhombohedral arrangement, the value of this ratio is always <2 (Figure 8e). Unlike SC, the flow encounters obstruction and changes direction in a rhombohedral arrangement of particles.

Simulations were also carried out for the 3-D rhombohedral geometry to study the influence of geometry orientation on velocity distribution. From Figure 7b it is quite clear that geometrical orientation does not induce a significant variation in overall drag force acting on the particle. However, results of SC and 1-D rhombohedral geometry indicate that there is a significant difference in the predicted flow field distribution for these two cases. Figures 4 and 8 also indicate that particle Reynolds number also plays a significant role in distribution of velocity inside the void. Except for the studies of Maier et al. (1998) and Magnico (2003), which report velocity distribution in a void at low Reynolds numbers, no information is available in the literature on how particle arrangement and particle Reynolds number influence velocity distribution. The predicted distribution of the z-velocity component is shown in Figure 9a for 1-D rhombohedral geometry at different particle Reynolds numbers. At the lowest Reynolds number (Re_p = 12.17), the z-velocity distribution exhibits a sharp peak and a shoulder. The predicted velocity distributions of rhombohedral arrange-

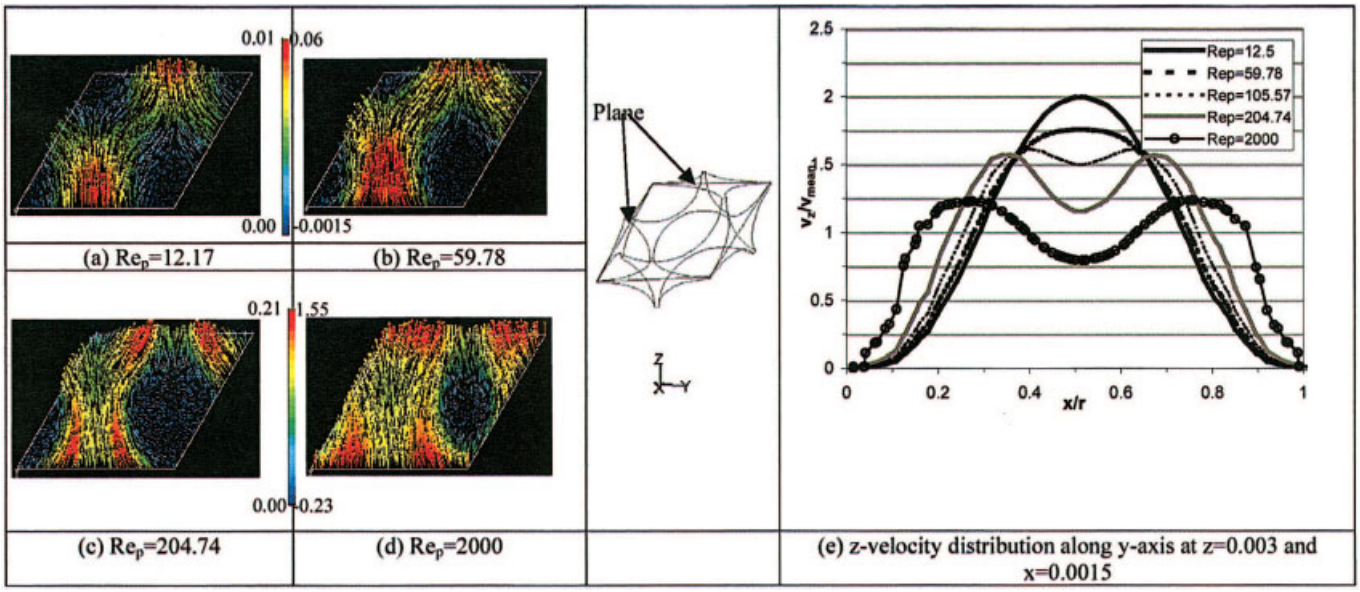

Figure 8. Velocity vectors and *z*-velocity distribution in rhombohedral cell at various particle Reynolds numbers.

ment are also similar to the results reported by Maier et al. (1998) and Magnico (2003). As the particle Reynolds number increases, the distribution broadens and distribution becomes bimodal. However, *z*-velocity distributions for 3-D rhombohedral geometry show different trends than those for the 1-D rhombohedral geometry (see Figure 9b). For 3-D rhombohedral geometry, a flatter velocity distribution was observed at low as well as high Reynolds numbers.

Distributions of the axial component of velocity within the interstitial space for SC, rhombohedral (1-D and 3-D), and FCC geometry were compared for $Re_p = 12.17$ in Figure 10a. For SC and 1-D rhombohedral geometry, the predicted velocity distribution curves indicate that there are large numbers of cells containing low-magnitude axial velocities. However, for 3-D rhombohedral and FCC geometry a flatter velocity distribution was observed. Sederman et al. (1997) experimentally measured velocity distribution within the packed beds using MRI. Their data for the particle Reynolds number of 16.1 are also shown in Figure 10a. The velocity distribution obtained from experimental data of randomly packed bed lies between the trends observed in different arrangements considered here. Similar trends were observed when distributions of one of the transverse velocity components (*x*-velocity) in the interstitial space was plotted (see Figure 10b).

Relative contributions of shear drag and form drag

CFD models provide detailed information about the flow field and pressure distribution within the considered domain. Such information might be used to understand and to quantitatively estimate relative contributions of shear drag and form drag in the overall pressure drop. Overall friction factor for the flow through packed bed may be defined as

$$\frac{\Delta P}{L} = af\frac{1}{2}\rho U_0^2 \tag{2}$$

where the left-hand side denotes pressure drop per unit length, f is the friction factor, U_0 is the superficial velocity, and a is the ratio of wetted area and volume of cell. From the CFD simulations of flow through unit cells, overall friction factors were calculated using Eq. 1 and simulated values of pressure drop per unit length. The predicted values of overall friction factor as a function of Reynolds number are shown in Figure 11. The well-known Ergun's equation can be used to estimate overall friction factor as

$$f = \frac{1}{2}\frac{(1-\varepsilon)}{\varepsilon^3}\left[E_1\frac{(1-\varepsilon)}{\mathrm{Re}} + E_2\right] \tag{3}$$

where E_1 and E_2 are Ergun's constants and ε is the bed porosity. This equation has been widely used to correlate the friction factor for the packed beds and the standard values of E_1 and E_2 are 150 and 1.75, respectively (Bird et al., 1960). Durst et al. (1987) critically analyzed the pressure drop in packed beds and suggested the value of E_1 as 182 instead of 150. The values of friction factor estimated using Eq. 2 and values of parameters suggested by Durst et al. (1987) are shown as solid continuous lines in Figure 11. It can be seen that the results obtained from the CFD simulations agree with those estimated using Eq. 2. It is interesting to note that the same values of E_1 and E_2 were able to estimate overall friction factors for all three packing arrangements considered in this work. Thus Eq. 2 seems to account for the influence of bed porosity on overall friction, irrespective of packing arrangement of the bed.

CFD simulations were then used to calculate viscous shear stress at the particle surfaces. The predicted value of viscous shear stress (area averaged) at the particle surfaces was used to obtain viscous friction factor f_s as

$$f_s = \frac{(\tau_w)_{sim}}{1/2\rho U_0^2} \tag{4}$$

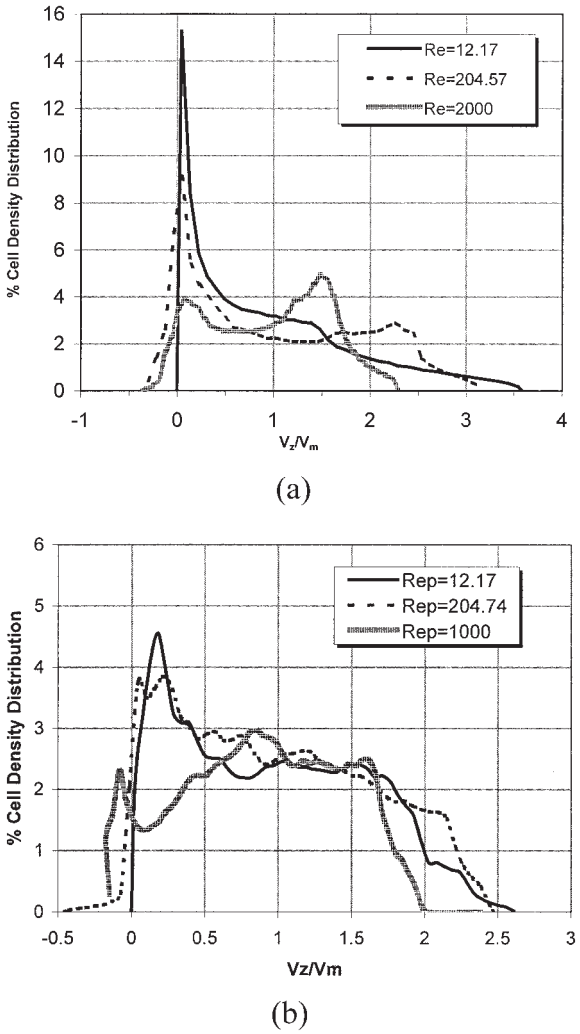

Figure 9. (a) Histograms of *z*-velocity distribution obtained from simulations of liquid flow in 1-D rhombohedral cell at different Re_p values; (b) histograms of *z*-velocity distribution obtained from simulations of liquid flow in 3-D rhombohedral cell at different Re_p values.

The variation of the ratio of viscous friction factor to the overall friction factor, with respect to particle Reynolds number, is shown in Figure 11 by dotted lines for the three particle arrangements. It can be seen that the relative contribution of surface shear stress (in overall pressure drop) is almost constant for the laminar regime. The value of this ratio is about 0.21 for the SC and FCC arrangements, whereas it is about 0.27 for the 1-D rhombohedral arrangement. The 3-D rhombohedral geometry shows the lowest ratio of viscous to total drag.

Effect of flow structure on heat transfer

The computational model was used to understand the influence of particle Reynolds number and particle arrangement on particle-to-fluid heat transfer in packed beds. The velocity distribution and recirculation within the interstitial space are expected to influence particle-to-fluid heat transfer. Path lines within the interstitial spaces of simple cubic and FCC arrangements are shown in Figure 12a. It can be seen that at the lowest higher particle Reynolds number (12.17), the path lines are almost parallel without any circulation. At higher particle Reynolds number (204.74), circulatory flow within the interstitial space was observed for the SC arrangement. Comparison of the path lines obtained for the SC and FCC arrangements clearly indicates that, unlike for the simple cubic arrangement, the flow impinges on the particle surface and changes direction several times within the interstitial space. For the SC arrangement, the bulk of fluid bypasses the particle surface. Simulated temperature fields for different Reynolds numbers for the SC

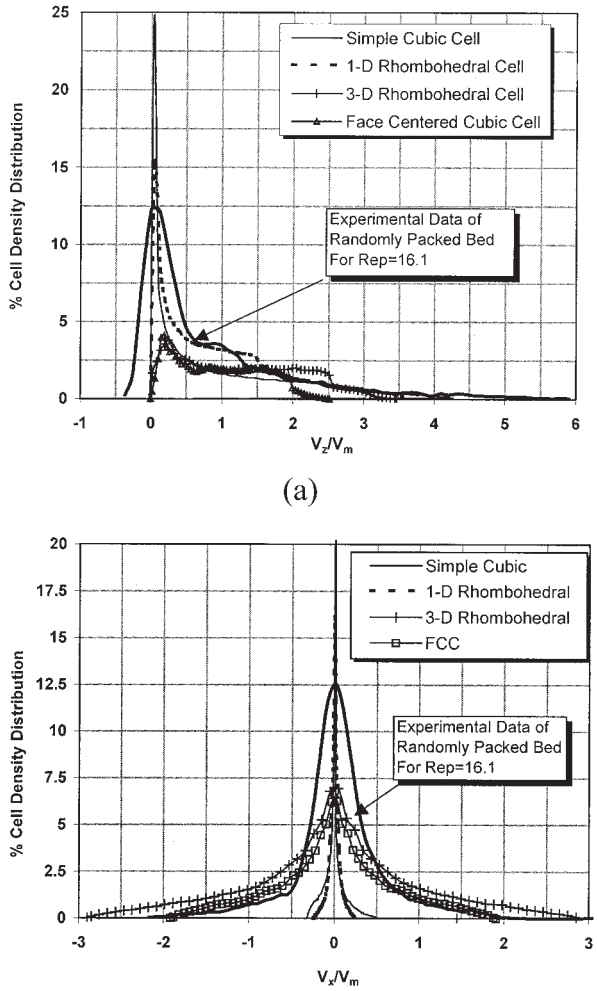

Figure 10. (a) Histograms of *z*-velocity distribution obtained from simulations of liquid flow in different unit cells at Re_p = 12.17 and experimental data of Sederman et al. (1997) in randomly packed bed (D = 4.7 cm; d_p = 5 mm, normalized density distribution); (b) histograms of *x*-velocity distribution obtained from simulations of liquid flow in different unit cells at Re_p = 12.17 and experimental data of Sederman et al. (1997) in randomly packed bed (D = 4.7 cm; d_p = 5 mm, normalized density distribution).

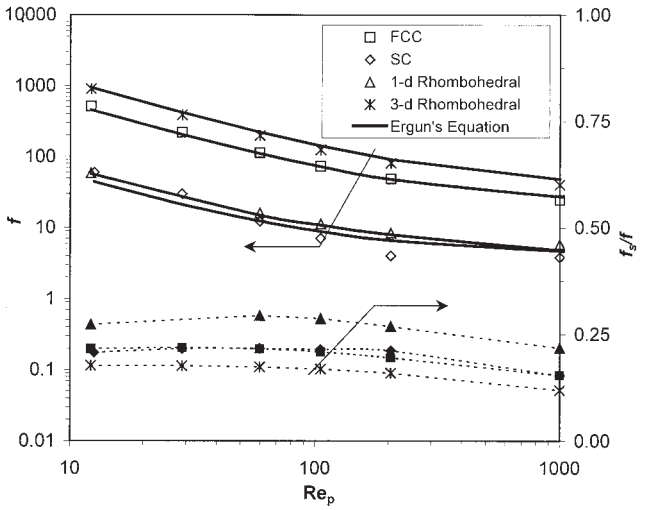

Figure 11. Simulated friction factor, shear drag, and Ergun equation.

Ergun's constant $E_1 = 180$, $E_2 = 1.75$; all open symbols indicate shear drag at the particle surface.

and FCC arrangements are also shown in Figure 12a. The interaction of circulatory flow and predicted temperature field is obvious from these results.

From the simulated values of enthalpy flux at the particle surface, the values of particle-to-fluid heat-transfer coefficients were calculated. The predicted values of Nusselt numbers for different values of the particle Reynolds numbers are shown in Figure 12b for SC and FCC arrangements. Values of Nusselt numbers estimated from the correlations proposed by Ranz (1952) and Wakao et al. (1979) are also shown in this figure. It can be seen that the predicted Nusselt number for the FCC arrangement shows reasonable agreement with the results of correlation of Ranz (1952). The predicted values of Nusselt number for the SC arrangement were found to be significantly lower than those obtained for the FCC arrangement. It should be noted that simulations for the SC arrangement were carried out with a different value of solid volume fraction. To separate the influence of solid volume fraction and particle packing arrangement, an additional simulation with the FCC arrangement with solid volume fraction of 0.5 (which is close to that used with the SC arrangement) was carried out. The predicted value of Nusselt number for this case was found to be slightly lower than that obtained for the FCC arrangement with higher volume fraction of solid but much higher than that obtained for the SC arrangement. The predicted overall friction factor, however, was much closer to that of the SC arrangement because the solid volume fractions are similar. Thus it can be concluded that the observed difference in the predicted Nusselt numbers of the simple cubic and FCC arrangements is primarily explained by the differences in flow structures within the interstitial space caused by different packing arrangements.

The unit-cell approach used in this work for understanding single-phase flow through voids in a packed bed may be extended to simulating gas–liquid flow through voids in a packed bed. Such a study will provide a sound basis for closure terms used in continuum models used to simulated gas–liquid flow through packed beds (see, for example, Gunjal et al., 2003).

Conclusions

A computational flow model using a "unit-cell" approach was developed to understand flow and heat transfer in packed beds of spheres. Different packing arrangements, such as simple cubic, rhombohedral (1-D and 3-D), and face-centered cubic, were considered. The model predictions were verified by comparing the simulation results with the published experimental and computational results. Predicted results showed excellent agreement with the experimental data of Suekane et al. (2003) for SC geometry. Simulated results showed good agreement with the analytical solution reported by Sangani and Acrivos (1982) at low volume fraction of solids for vanishing particle Reynolds number. The results of the present work also showed good agreement with the results obtained by Hill et al. (2001a) with lattice–Boltzmann simulation and with the results of Dhole et al. (2004) over a broad range of particle Reynolds numbers. It was found that the average drag force on particles is not significantly affected by the specific particle arrangement as long as solid volume fraction is the same.

The validated CFD model was used to understand the influence of particle Reynolds number and particle arrangement on velocity distribution within the interstitial space. In a laminar flow regime, the predicted magnitude of dimensionless maximum velocity was found to increase with the particle Reynolds number. However, for turbulent flow regime, the magnitude of dimensionless maximum velocity was almost independent of the particle Reynolds number and much lower than that observed with the laminar flow regime. Velocity distribution in 1-D rhombohedral geometry was found to be more sensitive than the 3-D rhombohedral geometry to the value of particle Reynolds number. The predicted velocity distributions for SC and 1-D rhombohedral geometries show sharp peaks, which indicate a large fraction of void volume with low velocities. However, for FCC and 3-D rhombohedral geometry, the predicted velocity distribution is significantly flat. Velocity distribution in a randomly packed bed (experimental results of Sederman et al., 1997) was found to lie between these two types (SC and 1-D rhombohedral; FCC and 3-D rhombohedral).

Total frictional resistance determined from the CFD simulations showed good agreement with the values estimated using the Ergun equation (with $E_1 = 182$ and $E_2 = 1.75$) for all three packing arrangements. The Ergun equation was found to overpredict the drag coefficient for the turbulent flow regime. The ratio of surface drag to overall drag was almost independent of particle Reynolds number in the laminar flow regime. The values of this ratio obtained for the SC and FCC arrangements were almost the same ($\sim$0.21). For the rhombohedral arrangement (1-D), the relative contribution of form drag was lower than that observed for the SC and FCC arrangements. The 3-D rhombohedral arrangement was found to offer maximum form drag.

The predicted values of Nusselt numbers for the FCC arrangement showed reasonable agreement with the correlations of the particle to fluid heat transfer in packed beds. The predicted values of Nusselt number for the SC arrangement were much lower than those obtained for the FCC arrangement. Unlike the FCC, where flow impinges on the obstructing particle and changes directions several times within the "unit cell," no impingement and direction changes occur in the SC arrange-

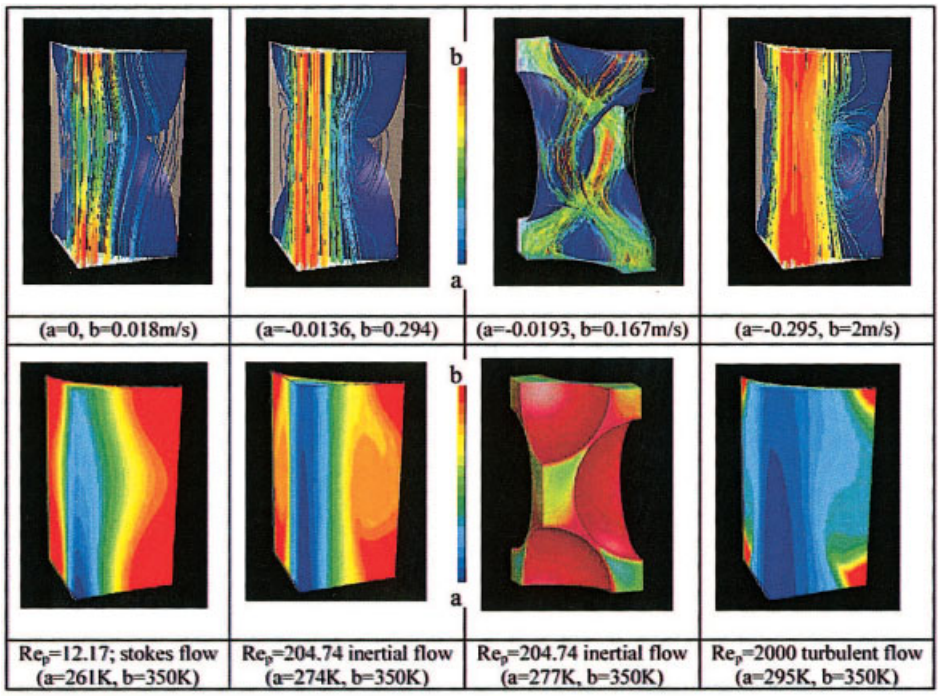

(a)

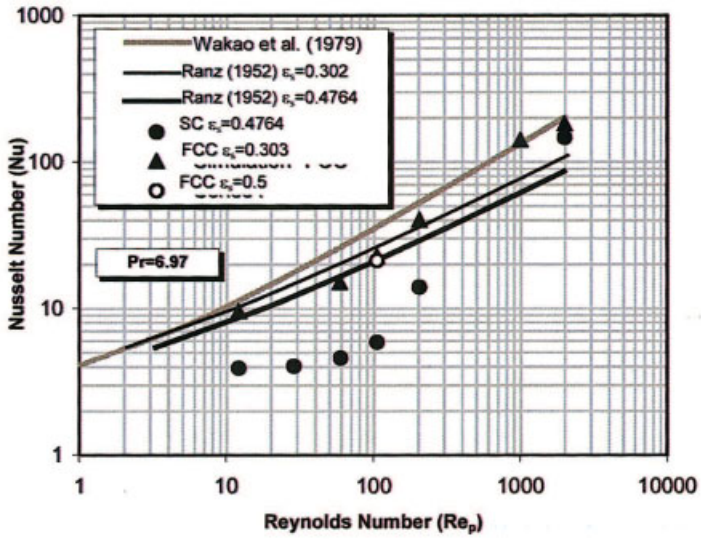

(b)

Figure 12. (a) Effect of the flow structure on temperature profile inside SC and FCC cells at various Re$_p$ values. (b) Local particle-to-fluid Nusselt number for cubical cell at various Re$_p$ values.

ment. This leads to significantly different path lines and velocity distribution and therefore the heat transfer.

The unit-cell approach was found to be useful for understanding the flow characteristics in a packed bed. The approach and models presented here may provide a basis for extending this study for understanding gas–liquid flow in packed beds.

Acknowledgments

One author (P. Gunjal) is grateful to the Council of Scientific and Industrial Research (CSIR), India for providing financial support. The authors thank Prof. Goverdhana Rao of the Indian Institute of Technology, Bombay for his help and also thank Prof. Suekane of the Tokyo Institute of Technology, Japan for providing experimental data.

Notation

a = cell specific surface area, m^2/m^3
E, $E2$ = Ergun's constant
D = column diameter, m
d_h = hydraulic diameter, m
f = total frictional factor
f_s = shear frictional factor

F = source for momentum equation
F = dimensionless drag force, $F_{\text{spheres}}/6\pi\mu U_0 d_p$
g_i = i-directional gravitational acceleration, m/s^2
h = heat transfer coefficient, W m^{-2} K^{-1}
k = thermal conductivity, W m^{-1} K^{-1}
k = turbulent kinetic energy, m^2/s^2
k_t = turbulent thermal conductivity, W m^{-1} K^{-1}
L = characteristics length of bed or cell, m
P = pressure, Pa
ΔP = pressure drop, Pa
q = heat flux, W
S_m = source term
t = time, s
T = temperature, K
u = velocity vector, m/s
U = superficial liquid velocity, m/s
V_c = volume of the cell
x, y, z = Cartesian coordinates, m

Greek letters

δ_{ij} = Kronecker delta
ε = turbulence energy dissipation rate, m^2/s^3
ε_b = bed voidage, m^3/m^3
ν = liquid viscosity, Pa·s
ν_t = turbulent eddy viscosity, Pa·s
ρ = liquid density, kg/m^3
τ_{ij} = shear stress, N/m^2
τ_w = wall shear stress, N/m^2

Dimensionless numbers

Nu = Nusselt number, hd_p/k
Pr = Prandlt number, $C_p\mu/K$
Pr$_t$ = turbulent Prandlt number, $C_p\mu_t/K$
Re = Reynolds number, $\rho U_0 d_p/m$
Re$_p$ = particle Reynolds number, $\rho U_0 d_p/\mu\varepsilon$

Literature Cited

Bird, R. B., W. E. Stewart, and E. N. Lightfoot, *Transport Phenomena*, Wiley, New York (1960).

Calis, H. P. A., J. Nijenhuis, B. C. Paikert, F. M. Dautzenberg, and C. M. van den Bleek, "CFD Modelling and Experimental Validation of Pressure Drop and Flow Profile in a Novel Structured Catalytic Reactor Packing," *Chem. Eng. Sci.*, **56**, 1713 (2001).

Chhabra, R. P., J. Comiti, and I. Machac, "Flow of Non-Newtonian Fluids in Fixed and Fluidized Bed," *Chem. Eng. Sci.*, **56**, 1 (2001).

Dixon, A. G., and M. Nijemeisland, "CFD as a Design Tool for Fixed-Bed Reactors," *Ind. Eng. Chem. Res.*, **40**, 5246 (2001).

Dhole, S. D., R. P. Chhabra, and V. Eswaran, "Power Law Fluid through Beds of Spheres at Intermediate Reynolds Numbers: Pressure Drop in Fixed and Distended Beds," *Chem. Eng. Res. Des.*, **82**(A6), 1 (2004).

Durst, F, R. Haas, and W. Interthal, "The Nature of Flows through Porous Media," *J. Non-Newtonian Fluid Mech.*, **22**, 169 (1987).

Freund, H., T. Zeiser, F. Huber, E. Klemm, G. Brenner, F. Durst, and G. Emig, "Numerical Simulations of Single Phase Reacting Flows in Randomly Packed/Fixed-Bed Reactors and Experimental Validation," *Chem. Eng. Sci.*, **58**, 903 (2003).

Gunjal, P. R., V. V. Ranade, and R. V. Chaudhari, "Liquid Phase Residence Time Distribution in Trickle Bed Reactors: Experiments and CFD Simulations," *Can. J. Chem. Eng.*, **81**, 821 (2003).

Hill, R. J., D. L. Koch, and A. J. C. Ladd, "Moderate-Reynolds-Number Flows in Ordered and Random Arrays of Spheres," *J. Fluid Mech.*, **448**, 243 (2001a).

Hill, R. J., D. L. Koch, and A. J. C. Ladd, "The First Effects of Fluid Inertia on Flows in Ordered and Random Arrays of Spheres," *J. Fluid Mech.*, **448**, 213 (2001b).

Jongen, T., "Simulation and Modeling of Turbulent Incompressible Flows," PhD Thesis, EPF Lausanne, Lausanne, Switzerland (1992).

Jolls, K. R., and T. J. Hanratty, "Transition to Turbulence for Flow through a Dumped Bed of Spheres," *Chem. Eng. Sci.*, **21**, 1185 (1966).

Kader, B., "Temperature and Concentration Profiles in Fully Turbulent Boundary Layers," *Int. J. Heat Mass Transfer*, **24**(9), 1541 (1993).

Kim, S. E., and D. Choudhury, "A Near-Wall Treatment Using Wall Functions Sensitized to Pressure Gradient," Proc. ASME FED, Separated and Complex Flows, **217**, ASME (1995).

Latifi, M. A., N. Midoux, A. Storck, and J. M. Gence, "The Use of Microelectrodes in the Study of Flow Regimes in a Packed Bed Reactor with Single Phase Liquid Flow," *Chem. Eng Sci.*, **44**, 2501 (1989).

Launder, B. E., and D. B. Spalding, "The Numerical Calculations of Turbulent Flows," *Comput. Methods Appl. Mech. Eng.*, **3**, 269 (1974).

Logtenberg, S. A., M. Nijemeisland, and A. G. Dixon, "Computational Fluid Dynamics Simulations of Fluid Flow and Heat Transfer at the Wall–Particle Contact Points in a Fixed Bed Reactor," *Chem. Eng. Sci.*, **54**, 2433 (1999).

Magnico, P., "Hydrodynamic and Transport Properties of Packed Bed in Small Tube-to-Sphere Diameter Ratio: Pore Scale Simulation Using an Eulerian and a Lagrangian Approach," *Chem. Eng. Sci.*, **58,** 5005 (2003).

Maier, R. S., D. M. Kroll, Y. E. Kutovsky, H. T. Davis, and R. S. Bernard, "Simulation of Flow through Bead Packs Using the Lattice–Boltzmann Method," *Phys. Fluids*, **10**, 60 (1998).

Martin, J. J., W. L. McCabe, and C. C. Monrad, "Pressure Drop through Stacked Spheres," C*hem. Eng. Prog.*, **47**(2), 91 (1951).

Natarajan, R., and A. Acrivos, "The Instability of the Steady Flow Past Spheres and Disks," *J. Fluid Mech.*, **254,** 323 (1993).

Nijemeisland, M., and A. G. Dixon, "Comparison of CFD Simulations to Experiment for Convective Heat Transfer in a Gas–Solid Fixed Bed," *Chem. Eng. J.*, **82**, 231 (2001).

Nijemeisland, M., and A. G. Dixon, "CFD Study in Fluid Flow and Wall Heat Transfer in a Fixed Bed of Spheres," *AIChE J.*, **50**(5), 906 (2004).

Ranz, W. E., "Friction and Transfer Co-efficient for Single Particles and Packed Beds," *Chem. Eng. Prog.*, **48**(8), 247 (1952).

Sangani, A. S., and A Acrivos, "Slow Flow through a Periodic Array of Spheres," *Int. J. Multiphase Flow*, **8**, 343 (1982).

Sederman, A. J., and L. F. Gladden, "Magnetic Resonance Visualization of Single- and Two-Phase Flow in Porous Media," *Magn. Reson. Imaging*, **19**, 339 (2001).

Sederman, A. J., M. L. Johns, A. S. Bramley, P. Alexander, and L. F. Gladden, "Magnetic Resonance Imaging of Liquid Flow and Pore Structure within Packed Bed," *Chem. Eng. Sci.*, **52**, 2239 (1997).

Seguin, D, A. Montillet, and J. Comiti, "Experimental Characterization of Flow Regimes in Various Porous media—I: Limit of Laminar Flow Regime," *Chem. Eng. Sci.*, **53**(21), 3751 (1998b).

Seguin, D., A. Montillet, J. Comiti, and F. Huet, "Experimental Characterization of Flow Regimes in Various Porous Media—II: Transition to Turbulent Regime," *Chem. Eng. Sci.*, **53**(22), 3897 (1998a).

Sørensen, J. P., and W. E. Stewart, "Computation of Forced Convection in Slow Flow through Ducts and Packed Beds—III. Heat and Mass Transfer in a Simple Cubic Array of Spheres," *Chem. Eng. Sci.*, **29**, 827 (1974).

Suekane, T., Y. Yokouchi, and S. Hirai, "Inertial Flow Structures in a Simple-Packed Bed of Spheres," *AIChE J.*, **49**, 1 (2003).

Tobis, J., "Influence of Bed Geometry in Its Frictional Resistance under Turbulent Flow Conditions," *Chem. Eng. Sci.*, **55**, 5359 (2000).

Wakao, N., S. Kaguei, and T. Funazkri, "Effect of Fluid Dispersion Coefficient on Particle-to-Fluid Heat Transfer Coefficients in Packed Beds—Correlations of Nusselt Numbers," *Chem Eng. Sci.*, **34**, 325 (1979).

Wolfstein, M., "The Velocity and Temperature Distribution of One-Dimensional Flow with Turbulence Augmentation and Pressure Gradient," *Int. J. Heat Mass Transfer*, **12**, 301 (1969).

Zeiser, T., M. Steven, H. Freund, P. Lammers, G. Brenner, F. Durst, and J. Bernsdorf, "Analysis of the Flow Field and Pressure Drop in Fixed-Bed Reactors with the Help of Lattice Boltzmann Simulations," *Philos. Trans. R. Soc. Lond. A*, **360**, 507 (2002).

Appendix

Governing equations

Reynolds-averaged Navier–Stokes equations for mass and momentum balance for incompressible Newtonian fluid are given by

$$\frac{\partial \boldsymbol{u}_i}{\partial x_i} = 0 \tag{A1}$$

$$\frac{\partial \boldsymbol{u}_i}{\partial t} + \frac{\partial (\boldsymbol{u}_i \boldsymbol{u}_j)}{\partial \boldsymbol{x}_j} = -\frac{1}{\rho}\frac{\partial P}{\partial \boldsymbol{x}_i} + \frac{\partial}{\partial \boldsymbol{x}_j}\left[(\nu + \nu_t)\left(\frac{\partial \boldsymbol{u}_i}{\partial \boldsymbol{x}_j} + \frac{\partial \boldsymbol{u}_j}{\partial \boldsymbol{x}_i}\right)\right] \tag{A2}$$

where $\boldsymbol{u}_i$ is the mean velocity in the i-direction and P is pressure. The turbulent kinematic viscosity ν_t is given as

$$\nu_t = C_\mu \frac{k^2}{\varepsilon} \tag{A3}$$

In this work, the standard k–ε model of turbulence was used. Transport equations for the turbulent kinetic energy k and the dissipation rate ε may be written as

$$\frac{Dk}{Dt} = \frac{\partial}{\partial \boldsymbol{x}_j}\left[\left(\nu + \frac{\nu_t}{\sigma_k}\right)\frac{\partial k}{\partial \boldsymbol{x}_j}\right] + G - \varepsilon$$

$$\because G = \nu_t \frac{\partial \boldsymbol{u}_i}{\partial \boldsymbol{x}_j}\left(\frac{\partial \boldsymbol{u}_i}{\partial \boldsymbol{x}_j} + \frac{\partial \boldsymbol{u}_j}{\partial \boldsymbol{x}_i}\right) \tag{A4}$$

$$\frac{D\varepsilon}{Dt} = \frac{\partial}{\partial \boldsymbol{x}_j}\left[\left(\nu + \frac{\nu_t}{\sigma_\varepsilon}\right)\frac{\partial \varepsilon}{\partial \boldsymbol{x}_j}\right] + \frac{\varepsilon}{k}(C_{1\varepsilon}G - C_{2\varepsilon}\varepsilon) \tag{A5}$$

Standard values of the parameters appearing in Eqs. A3 to A5 were used [$C_{1\varepsilon} = 1.44$, $C_{2\varepsilon} = 1.92$, $C_\mu = 0.09$, $s_k = 1.0$, and $s_e = 1.3$; from Launder and Spalding (1974)]. For turbulent flow simulations, various wall functions [standard wall function of Launder and Spalding (1974)], enhanced wall function (Jongen, 1992; Kader, 1993; Wolfstein, 1969), and the nonequilibrium wall function of Kim and Choudhury (1995) were used. However, the predicted flow field was not significantly influenced by the choice of wall functions.

The energy conservation equation may be written as

$$\frac{\partial(\rho h)}{\partial t} + \boldsymbol{\nabla} \cdot (\rho \boldsymbol{u}_i h) = (k + k_t)\boldsymbol{\nabla}^2 T \tag{A6}$$

where h is enthalpy, k is thermal conductivity, and k_t is the turbulent thermal conductivity. The first term in the right-hand side is of the effective conductive heat flux (molecular and turbulent). The turbulent thermal conductivity is given by

$$k_t = \frac{C_p \mu_t}{\mathrm{Pr}_t} \tag{A7}$$

Boundary conditions

To model the unit cell as a representative piece of a packed bed, periodic boundary conditions were implemented at all the faces of the unit cell through which flow occurs. Here translational periodic boundary condition is used in which all variables except pressure at periodic planes are identical. For a desired particle Reynolds number, superficial velocity and mass flow rates were calculated based on the considered geometry. However, pressure is not periodic; instead the pressure drop is periodic. The local pressure gradient can therefore be decomposed into two parts: the gradient of a periodic component and the gradient of a linearly varying component. The linearly varying component of the pressure results in a force acting on the fluid in the momentum equations. Because the value of pressure gradient is not known a priori, it must be iterated until the specified mass flow rate is achieved in the computational model. This correction of pressure gradient occurs in the pressure correction step of the SIMPLE algorithm, where the value of pressure gradient is updated based on the difference between the desired mass flow rate and the actual one. In the present work, we have used an underrelaxation parameter of 0.5 and 2 internal iterations to ensure the desired mass flow rate through the periodic cell.

While carrying out experiments of flow through an array of spheres, Suekane et al. (2003) closed the side faces of their cubical unit cell. The effect of closing the side faces (by specifying boundary condition as impermeable no-slip walls) as against the open, periodic faces was computationally studied.

For all the vertical faces bounding the solution domain, symmetry boundary conditions were implemented (normal velocity and all other normal gradients were set to zero). A no-slip boundary condition was implemented on all the impermeable walls (curved solid surfaces in Figures 1a–c). For carrying out heat transfer simulations, a constant-temperature (350 K) boundary condition was specified at all the particle surfaces and upstream bulk temperature was specified as 300 K. Heat transfer from particles to the fluid was calculated as

$$q = hA(T_w - T_b) = -k_f\left(\frac{\partial T}{\partial n}\right)_{wall} \tag{A8}$$

where n is the normal coordinate normal to the wall and k_f is the thermal conductivity of fluid. Temperature gradients obtained from simulations were used to calculate the particle-to-fluid heat-transfer coefficient.

Manuscript received Jun. 13, 2003, and revision received May 29, 2004.